



ORIGINAL ARTICLE

Optimum design of precast and prestressed beams with focus on CO₂ emission reduction

Projeto ótimo de vigas pré-fabricadas e protendidas com foco na redução da emissão de CO₂

Matheus Henrique Morato de Moraes^a

Wanderlei Malaquias Pereira Junior^b

Sylvia Regina Mesquita de Almeida^c

Geraldo Magela Gonçalves Filho^b

Rebeca Freitas Vasconcelos^d



^aUniversidade Federal de São Carlos – UFSCar, Civil Engineering Graduate Program, São Carlos, SP, Brasil

^bUniversidade Federal de Catalão – UFCAT, Civil Engineering Department, Catalao, GO, Brasil

^cUniversidade Federal de Goiás – UFG, School of Civil and Environmental Engineering, Goiânia, GO, Brasil

^dInstituto Federal do Tocantins – IFTO, Civil Engineering Department, Palmas, TO, Brasil

Received 24 March 2022

Accepted 05 October 2022

Abstract: Among the main contributors to CO₂ emissions on the ozone layer, the construction industry contributes with a significant portion. This emission is generated largely by applying concrete construction systems and their variations. Therefore, it is important to use tools that allow the development of projects which mitigate the effects of harmful gas emissions into the atmosphere. Thus, this study applied an optimization algorithm called Firefly Algorithm (FA) to design precast and prestressed rectangular beams focusing on reducing CO₂ emissions in the structural design phase. The Objective Function (OF) was defined as the total weight of CO₂ emitted in each construction phase (production, transportation, and placement) and the structural design constraints are based on the design criteria established in ABNT NBR 6118. The problem optimization's variables are geometric properties and mechanical beam's conditions, where the beam height, beam width, the proportion of height generates prestressing eccentricity, and the proportion of prestressing load were considered as design variables. Ten beams were analyzed, with different loadings, where each of these beams was submitted to the optimization process thirty times. For the proposed conditions, the ten beams had an average CO₂ emission of 3282.59 kg, maximum and minimum carbon emission of 3630.52 kg and 2910.67 kg, respectively. The study resulted in a feasibility rate higher than 90%, showing that the optimization tool was efficient in the structural design phase focusing on sustainability. Concerning carbon emission, it is possible to verify a relationship between the increase of emission and the load since element with greater inertia tend to emit a greater amount of CO₂. It was also possible to determine a regression between carbon emission and beam load.

Keywords: sustainability, CO₂ emission, optimization, precast concrete, prestressed concrete.

Resumo: Entre os principais responsáveis pelas emissões de CO₂ na camada de ozônio, a indústria da construção civil contribui com uma parcela significativa. Esta emissão é gerada em grande parte pela aplicação de sistemas de construção em concreto e suas variações. Portanto, é importante o uso de ferramentas que permitam o desenvolvimento de projetos que mitiguem os efeitos das emissões de gases nocivos para a atmosfera. Desse modo, este estudo aplicou um algoritmo de otimização chamado *Firefly Algorithm* (FA) para projetar vigas retangulares pré-fabricadas e protendidas com foco na redução da emissão de CO₂ na fase de projeto estrutural. A Função Objetiva (FO) foi definida como o peso total de CO₂ emitido em cada fase de construção (produção, transporte e montagem) e as restrições de projeto estrutural são baseadas nos critérios de projeto estabelecidos na ABNT NBR 6118. As variáveis do problema de otimização tratam de propriedades

Corresponding author: Matheus Henrique Morato de Moraes. E-mail: matheus.h.h@hotmail.com

Financial support: This study was financed in part by the Coordenação de Aperfeiçoamento de Pessoal de Nível Superior – Brasil (CAPES) – Finance Code 001.

Conflict of interest: Nothing to declare.

Data Availability: The information required to reproduce findings of this study is reported in the paper. Other data such as computer codes will be made available by the corresponding author upon reasonable request.



This is an Open Access article distributed under the terms of the Creative Commons Attribution License, which permits unrestricted use, distribution, and reproduction in any medium, provided the original work is properly cited.

geométricas e condições mecânicas da viga, onde foram consideradas variáveis de projeto a altura da viga, espessura da viga, a proporção de altura que gera excentricidade de protensão, e a proporção da força de protensão. Foram analisadas dez vigas, com diferentes carregamentos, onde cada uma dessas vigas foi submetida ao processo de otimização trinta vezes. Para as condições propostas, as dez vigas apresentaram uma emissão de CO₂ médio de 3282.59 kg, emissão de carbono máximo e mínimo de 3630.52 kg e 2910.67 kg, respectivamente. O estudo resultou em uma taxa de factibilidade superior à 90%, mostrando que a ferramenta de otimização foi eficiente na fase de projeto estrutural com foco na sustentabilidade. Em relação a emissão de carbono, é possível verificar uma relação entre o aumento da emissão e o carregamento visto que peças com maior inércia tendem a emitir uma maior quantidade de CO₂. Ainda foi possível determinar uma regressão entre a emissão de carbono e o carregamento da viga.

Palavras-chave: sustentabilidade, emissão de CO₂, otimização, concreto pré-fabricado, concreto protendido.

How to cite: M. H. M. Moraes, W. M. Pereira Junior, S. R. M. Almeida, G. M. Gonçalves Filho, and R. F. Vasconcelos, "Optimum design of precast and prestressed beams with focus on CO₂ emission reduction," *IBRACON Struct. Mater. J.*, vol. 15, no. 6, e15606, 2022, <https://doi.org/10.1590/S1983-41952022000600006>

1 INTRODUCTION

Among the main contributors to the emission of CO₂ on the ozone layer, the construction industry contributes with a significant portion [1]. This emission is largely generated by concrete structural systems and their variations, whereas in 2020, the construction industry alone was responsible for approximately 38% of all global CO₂ emissions [2]. In addition, the cement industry produces approximately 5% of global greenhouse gas emissions [3]. Therefore, using tools that allow the development of projects which mitigate the effects of greenhouse gas emissions is essential.

As every economy's sector, civil construction has been going through several changes which involve the insertion of new technologies and a new view on the rational use of materials [4]–[6]. From this perspective, precast construction offers favorable conditions to achieve these new guidelines for the sector. This model has characteristics such as fast execution, high-quality control, optimization of shapes of elements and production planning, rational use of materials, and versatility [7], [8]. Besides the fact narrated above, the prefabrication technology is already consolidated worldwide and has solutions for producing several structural models such as slabs, beams, columns, and masonry walls.

In terms of precast elements design, the biggest challenge for the designer is determining the optimal dimensions and characteristics of the structural element. In a conventional project, these characteristics are estimated intuitively and based on experience [9]. Then, the design of this structure's type becomes an iterative process of searching for the characteristics which satisfy the design criteria established by existing standards. In a corporate structural design environment, this analysis model may be inefficient, and the success rate is based entirely on the designer's experience.

Therefore, computational intelligence based on numerical analysis tools can become an ally to improve efficiency in the structure design. Such analysis tools are usually based on an optimization problem in which one wishes to determine a given function's variables, minimizing or maximizing. In structural designs, most of the time, what is sought is to optimize the cost or the total weight of the structure [10].

In the field of structural design several optimization applications can be found, such as, the researches of Al-Gahtani et al. [11], Alberio et al. [12], Navarro-Rubio et al. [8], Castilho [13], and Castilho et al. [14] that applied optimization concepts to reduce the cost and weight of precast elements. Other applications in the field of structural engineering can be observed in Azad et al. [10] applied an optimization process for steel trusses under dynamic excitation. Juliani and Gomes [15] optimized reinforced concrete (RC) frames, with genetic algorithms, such as Pires and Silva [16] which optimized slender RC columns subject to biaxial bending. Cardoso et al. [17] evaluated the static and dynamic wind effect applying structural optimization of concrete plane frames. Christoforo et al. [18] and Moraes et al. [19] applied optimization for wood truss roof structures.

In the field of sustainability, Yücel et al. [20] applied a generation of sustainable models with multi-objective optimization to design RC structures with a focus on minimizing the cost and CO₂ emission. Yu et al. [21] optimized the embodied energy and cost of RC beams under blast load. Yu et al. [22] evaluated the Life cycle embodied energy analysis of RC structures considering chloride-induced corrosion in seismic regions.

Given the possibility to apply structural optimization, this work aims to develop optimization models based on computational intelligence for application in the design of precast and prestressed concrete beams that focus on reducing CO₂ emissions. In this work, the design recommendations are based on the Brazilian standards ABNT NBR 14861 [23], ABNT NBR 9062 [24], and ABNT NBR 6118 [25].

This paper is developed in 6 sections. Sections 2 and 3 refer to the assembly of the optimization problem for precast and prestressed concrete. Section 4 presents the procedure for designing and analyzing the results. Sections 5 and 6 present the results, discussions, and conclusions regarding this research.

2 DESIGN CRITERIA FOR PRECAST AND PRESTRESSED BEAMS

This section presents the design criteria for constructing an optimal design problem for precast and prestressed concrete elements are presented.

2.1 Transient phases and mechanical properties of concrete

The first observation regarding the design of precast and prestressed elements is the consideration of transient phases in the design process. The transient phase is inherent to precast concrete and is considered an intermediate stage to the use of the structure and can become critical, leading the element to a limit [26]. According to Lewick [27] and Krahl et al. [28], the different phases must be considered, such as manufacturing in the course, storage, transport, and placement of the elements.

A concern of these transitory phases is the determination of the efforts acting on the structure that are usually different from those that occur in service situations. An example would be lifting a precast concrete beam where the lifting and transportation situation could modify the diagram of efforts of the element according to Figure 1.

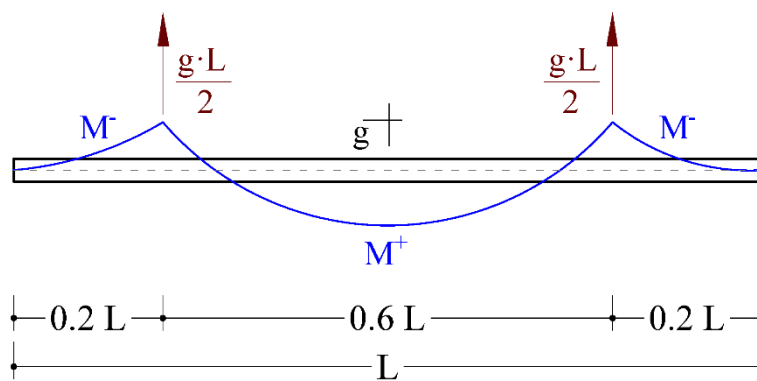


Figure 1. Example of beam and panel lifting [29].

Another important factor in the transient phase is the determination of the mechanical properties of concrete at an age j less than 28 days. Therefore, in these stages, the concrete properties, such as the characteristic compressive strength at age j ($f_{ck,j}$), can be evaluated according to Equations 1 and 2.

$$f_{ck,j} = \beta_1 \cdot f_{ck} \tag{1}$$

$$\beta_1 = e^{s \cdot \left(1 - \sqrt{\frac{28}{t}}\right)} \tag{2}$$

Where f_{ck} is the characteristic strength of concrete at 28 days, $f_{ck,j}$ is the characteristic strength of concrete at j days, t is the effective age of concrete, in days, s is a coefficient that varies according to the type of concrete, being adopted $s = 0.38$ for cement concrete CP III and IV, $s = 0.25$ or cement concrete CP I and II, and $s = 0.20$ for cement concrete CP V-ARI.

The properties derived from f_{ck} , such as tensile strength and modulus of elasticity, can be evaluated as described in sections 8.2.5 and 8.2.8 of ABNT NBR 6118 [25].

2.2 Initial prestressing stress

For prestressed concrete elements, it is necessary to determine the initial stress (σ_{pi}) in the prestressing strands. For pre-tensioned elements, normal relaxation (NR) and low relaxation (LR) steels are given in Equations 3 and 4, respectively.

$$\sigma_{pi} \leq \begin{cases} 0.74 \cdot f_{ptk} \\ 0.87 \cdot f_{pyk} \end{cases} \quad (3)$$

$$\sigma_{pi} \leq \begin{cases} 0.74 \cdot f_{ptk} \\ 0.82 \cdot f_{pyk} \end{cases} \quad (4)$$

Where f_{ptk} is the characteristic rupture stress of the steel, f_{pyk} is the characteristic yield stress of the steel, and σ_{pi} is the stress in the strand in the prestressing operation.

2.3 Prestressing losses

Another relevant observation in the design and verification of precast and prestressed concrete elements is the losses of prestressing load. These losses can be classified as time (immediate or progressive losses, see Table 1) and the cause (anchorage, steel relaxation, concrete creep, shrinkage, concrete shortening).

Table 1. Prestressing losses.

Type of loss	Classification by time
Anchorage	Immediate
Steel relaxation	Immediate
Strain immediate	Immediate
Shrinkage of concrete	Progressive
Concrete creep	Progressive
Steel relaxation with time	Progressive

Prestressing losses can be estimated or calculated. The details of prestressing losses are described in item 9.6.3 of ABNT NBR 6118 [25]. The immediate prestressing losses for precast and prestressed systems can be subdivided into: (a) attrition; (b) anchorage slippage; (c) immediate strain; (d) initial steel relaxation; and (e) initial concrete shrinkage, and the latter can be disregarded in the case of factory production since the time between the transfer of the prestressing load to the system and the concreting is small. The progressive losses can be divided into three groups: (a) concrete shrinkage; (b) concrete creep; and (c) steel relaxation.

As presented in Table 1, prestressing losses can be immediate (ΔP_{ime}) and progressive (ΔP_{pro}), so the prestressing load as a function of time ($P(t)$) is calculated based on Equation 5, where the prestressing losses reduced the initial load (P_i).

$$P(t) = P_i - \sum \Delta P_{ime} - \sum \Delta P_{pro} \quad (5)$$

The simplified process for iteration of the prestressing losses was considered. Thus, according to item 9.6.3.4.2 of ABNT NBR 6118 [25], the calculation of the simultaneous loss of concrete creep and shrinkage and steel relaxation is given by Equation 6.

$$\Delta \sigma(t, t_0) = \frac{\varepsilon_{cs}(t, t_0) \cdot E_p - \alpha_p \cdot \sigma_{c, p0g} \cdot \phi(t, t_0) - \sigma_{p0} \cdot \chi(t, t_0)}{\chi_p + \chi_c \cdot \alpha_p \cdot \eta \cdot \rho_p} \quad (6)$$

Where $\varepsilon_{cs}(t, t_0)$ is shrinkage at instant t , discounted the shrinkage that occurred up to instant t_0 , E_p is the modulus of elasticity of the prestressing steel, α_p is the ratio between the modulus of elasticity of steel (E_s) and concrete (E_c) (see Equation 10), $\sigma_{c, p0g}$ is stress in the concrete adjacent to the resulting strand, $\phi(t, t_0)$ is creep coefficient of concrete at instant t prestressing and dead load applied at instant t_0 (see Equation 9), σ_{p0} is the stress in the active reinforcement due to prestressing and dead load, ρ_p is the prestressed tendon reinforcement ratio (see Equation 12), $\chi(t, t_0)$ is the steel creep coefficient (see Equation 7 and Equation 8), and η is a geometric coefficient that depends on the eccentricity of the resultant cable relative to the barycenter of the concrete section (e_p), cross-sectional area of the concrete (A_c), and I_c is the central moment of inertia of the concrete section (see Equation 11).

$$\chi(t, t_0) = -\ln [1 - \psi(t, t_0)] \tag{7}$$

$$\chi_p = 1 + \chi(t, t_0) \tag{8}$$

$$\chi_c = 1 + 0.5 \cdot \phi(t, t_0) \tag{9}$$

$$\alpha_p = \frac{E_p}{E_{ci}} \tag{10}$$

$$\eta = 1 + e_p^2 \cdot \frac{A_c}{I_c} \tag{11}$$

$$\rho_p = \frac{A_p}{A_c} \tag{12}$$

Where $\psi(t, t_0)$ is the relaxation coefficient of steel at instant t for prestressing and dead load mobilized at instant t_0 , ρ_p is the geometric ratio of prestressing tendon reinforcement, and A_p is the cross-sectional area of the resultant active reinforcement cable.

3 OPTIMAL DESIGN CONSTRAINTS

From the point of view of optimization theory, the engineering sizing process is characterized as a constrained optimization procedure. It is necessary to evaluate constraints that delimit the search space during the method. These constraints or limitations are related to the physical feasibility of the structural element, Ultimate Limit State (ULS) constraints, and Serviceability Limit State (SLS) constraints. This section presents the design constraints for a prestressed precast concrete beam.

3.1 Verification of normal stresses

In some stages of the prestressed precast concrete beam design the structural element must satisfy the normal stresses established in Table 2.

Table 2. Conditions, combinations, and limits for verification of normal stresses [25].

Conditions to be verified		Limits	
		σ_c	σ_t
In construction			
In service	Prestressed concrete level 2 (limited prestressing)	SLS-CF	$0.70 \cdot f_{ckj}$
		FC ¹	$1.20 \cdot f_{ct,m}$
		SLS-D	0
		QPC ¹	

¹QPC – Quasi-Permanent load Combination, FC - Frequent load Combination. σ_c - Stress at the compressed region, σ_t - Stress at the tensioned region, SLS-CF - Limit state for crack formation, and SLS-D- limit state for decompression

Equations 13 and 14 are employed to calculate the stresses, representing the normal stresses in the section's bottom (σ_b) and top (σ_t) fibers, respectively.

$$\sigma_b = \frac{P(t)}{A_c} - \frac{P(t) \cdot e_p}{W_i} - \delta_{gi} \cdot \sum_{i=1}^{n_g} \frac{M_{gi}}{W_s} - \delta_{q1} \cdot \frac{\Psi_{q1} \cdot M_{q1}}{W_i} - \delta_{q2} \cdot \frac{M_{q2}}{W_i} \tag{13}$$

$$\sigma_t = \frac{P(t)}{A_c} - \frac{P(t) \cdot e_p}{W_s} + \delta_{gi} \cdot \sum_{i=1}^{n_g} \frac{M_{gi}}{W_s} + \delta_{q1} \cdot \frac{\Psi_{q1} \cdot M_{q1}}{W_s} + \delta_{q2} \cdot \frac{M_{q2}}{W_s} \tag{14}$$

Where $P(t)$ is the prestressing load for each analyzed stage, corresponding to an age t of the concrete, M_{gi} is the i -th dead load bending moment; M_{q1} and M_{q2} represent the live load moments arising from the in-service use and assembly process of the system. A_c and W represent the geometric properties of the cross-section.

In addition, the verification of normal stresses in transient phases may or may not account for the loading on the structure. Table 3 presents this summary of the coefficients used for each type of loading for each structural design stage.

Table 3. Coefficients δ_{g1} , δ_{q1} , and Ψ_{q1} in each analysis stage [9].

Stage		δ_{g1}	δ_{g2}	δ_{g3}	δ_{q1}	δ_{q2}	Ψ_{q1}
Construction	Cutting of the strands	1	0	0	0	0	0
	Lifting and transport in the industry	β_a	0	0	0	0	0
	Lifting and transport on the construction site	β_a	0	0	0	0	0
	Assembly	1	1	0	0	1	0
	Coating	1	1	1	0	1	0
SLS	In service	1	1	1/0	1	0	Ψ_{SLS}

Where the parameter Ψ_{SLS} corresponds to the reduction factor in combinations in service (Ψ_1 for frequent combination and Ψ_2 for quasi-permanent load combination) and β_a is the dynamic amplification coefficient for situations in which it is necessary to consider the vibration effects in the structural element. More details can be verified in ABNT NBR 9062 [30]. The parameter δ indicates the existence or not of the load at that stage, being g and q identification for dead and live loads, respectively.

The stress constraints include the ultimate limit state (ULS) when, for example, the verification is performed during prestressing, called here strand shear. In the verification in service, the checks correspond to the Service Limit State (SLS).

3.2 Deflection Verification (SLS)

These constraints ensure that the structural element works in service. In the case of this work, the verification used is deflection. Therefore, three verifications are required for the Serviceability Limit State of Excessive Deformations (SLS-DEF). The first two are related to the sensory acceptability of the structural element. These relate to visible displacements in structural elements (Equation 15) and vibrations felt on the floor (Equation 16).

$$(f_{p6} + f_{g1})(1 + \phi_{(T_1, \infty)}) + f_{g2}(1 + \phi_{(T_4, \infty)}) + f_{g3}(1 + \phi_{(T_5, \infty)}) + \psi_A \cdot f_q \leq \frac{L}{250} \tag{15}$$

$$f_q \leq \frac{L}{350} \tag{16}$$

Where ψ_A is the weighting coefficient for live load; T_1 is the time relative to cutting the strands; T_2 is the time relative to performing the cover or placing other dead loads in the system; and T_5 corresponds to the creep coefficient at each time informed.

The last verification of deflection refers to the manufacturing tolerance of precast elements, aiming at their linearity. For calculation purposes, positive and negative displacements should be considered, according to Equation 17.

$$f_p + f_{g1} \leq \pm \frac{L}{1000} \tag{17}$$

3.3 Bending strength section verification (ULS)

This section presents the requirements for evaluating the cross-section regarding the resistant section requirements. The resistant capacity relative to the compression struts and the resistant bending moment will be evaluated.

For verification of shear capacity, how to prescribed by ABNT NBR 6118 [25], it is necessary to calculate the design resistant shear load (V_{Rd2}) given according to Equation 18:

$$V_{Rd2} = 0.27 \cdot \alpha_{v2} \cdot f_{cd} \cdot b_w \cdot d \tag{18}$$

Where V_{Rd2} is the design resistant shear load, relative to the failure of the compressed concrete strut; f_{cd} is the compressive design strength of concrete; b_w and d are geometric properties of the section; α_{v2} is given by Equation 19. It is worth noting that this formulation is applicable to reinforced concrete and prestressed concrete elements.

$$\alpha_{v2} = 1 - \frac{f_{ck}}{250} \tag{19}$$

To determine the flexural strength section in the ULS of the prestressed elements, the principle of balance of loads is assumed in the cross-section, as shown in Figure 2.

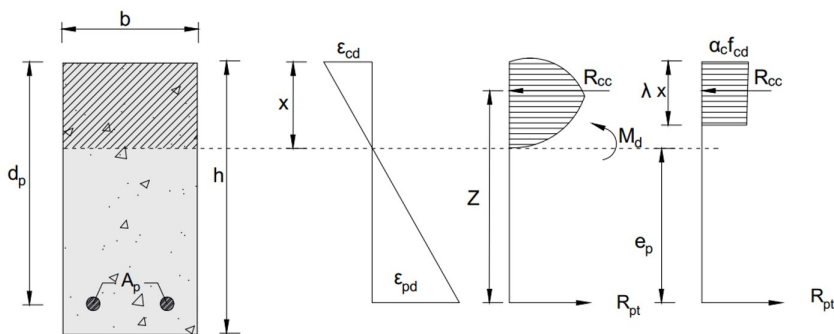


Figure 2. Stress-strain diagram of the rectangular section.

Based on the stress-strain diagram shown in Figure 2: b , d_p , and h are the width, effective depth, and height of the beam; ϵ_{cd} and ϵ_{pd} are the specific strains of the concrete and tendon; λ is the height value of the simplified rectangular diagram of the compressed concrete distribution; x is the neutral axis of the rectangular section; α_c is the multiplier value of the maximum compressive stress (Rüsch effect) for the concrete; e_p is the eccentricity of the resultant cable in relation to the barycenter of the concrete section; A_p is the area of the prestressed tendon reinforcement, M_d is the design bending moment of the section; f_{cd} is the design concrete compressive strength, Z is the lever arm of the compressive strength in concrete (R_{cc}) and tensile strength in prestressed tendon reinforcement (R_{pt}). The load R_{cc} is obtained by the product of the area of the compressed concrete ($A_c = \lambda \cdot x \cdot b$) and the acting stress in the concrete ($\sigma_{cd} = \alpha_c \cdot f_{cd}$) and the load R_{pt} is obtained by the product of the area of the tendon reinforcement (A_p) and the design stress of the prestressed tendon reinforcement (f_d), being presented in Equations 20 and 21, respectively.

$$R_{cc} = \alpha_c \cdot f_{cd} \cdot \lambda \cdot x \cdot b \tag{20}$$

$$R_{pt} = A_p \cdot f_d \tag{21}$$

The position of the neutral axis (x) is given by the Equation 22:

$$x = \frac{A_p \cdot f_d}{\alpha_c \cdot f_{cd} \cdot \lambda \cdot b} \tag{22}$$

The resistant bending moment (M_{Rd}) of the section is given by Equation 23:

$$M_{Rd} = A_p \cdot f_d \cdot \left(d_p - \frac{\lambda}{2} \cdot x \right) \tag{23}$$

Although determining the resistant bending moment is similar to the calculation model used in reinforced concrete, it is worth noting that in prestressed elements, the tendon suffers an initial prestressing that should be considered when

calculating the steel reinforcement stress (f_d). Therefore, the active tendon reinforcement level strain must consider the following portions presented in Equation 24.

$$\epsilon_{pd,total} = \epsilon_{pd,ini} + \epsilon_{pd,elo} + \epsilon_{pd,ult} \tag{24}$$

Where $\epsilon_{pd,total}$ is the strain of initial elongation of the tendon reinforcement; $\epsilon_{pd,inic}$ is the strain of initial elongation of the tendon reinforcement; $\epsilon_{pd,enc}$ is the strain due to shortening of the concrete; and $\epsilon_{pd,ult}$ is the strain corresponding to the portion of elongation of the tendon reinforcement in the ULS. To determine the strains $\epsilon_{pd,ini}$, $\epsilon_{pd,elo}$, and $\epsilon_{pd,ult}$ are presented in Equations 25, 26, and 27, respectively.

$$\epsilon_{pd,ini} = \frac{\sigma_{pd}}{E_p} = \frac{P_d}{E_p \cdot A_p} \tag{25}$$

$$\epsilon_{pd,elo} = \frac{\sigma_{cpd}}{E_c} = \frac{1}{E_c} \cdot \left(\frac{P_d}{A_c} + \frac{P_d \cdot e_p^2}{I_c} \right) \tag{26}$$

$$\epsilon_{pd,ult} = \epsilon_{cd} \cdot \frac{(d_p - x)}{x} \tag{27}$$

Where σ_{pd} is the stress in the prestressing tendon reinforcement; P_d is the prestressing load; σ_{cpd} is the concrete stress at the level of the center of gravity of the prestressing tendon reinforcement due to the P_d load; E_c is the modulus of elasticity of the concrete; E_p is the modulus of elasticity of the prestressing tendon reinforcement; and I_c is the moment of inertia of the concrete section.

4 METHODS

This section describes the procedures for building the algorithm for the optimization problem focused on minimizing the carbon footprint of a concrete beam, precast, prestressed, and straight cables. All the implementation of the optimization method and the verification processes of the concrete element were done using the Python language and the free Google Colaboratory environment.

4.1 Characteristics to build the objective function

Equation 31 is the Objective Function (OF) of the optimization problem. In this function, the dimensions of beam height (h), beam width (b), the proportion of height that generates prestressing eccentricity (e_p), and the proportion of prestressing load (P_i) are considered design variables. The design variables (\mathbf{x}) and the cross-section model of the full span beam (L) and active tendon reinforcement area (A_p), are presented in Figure 3.

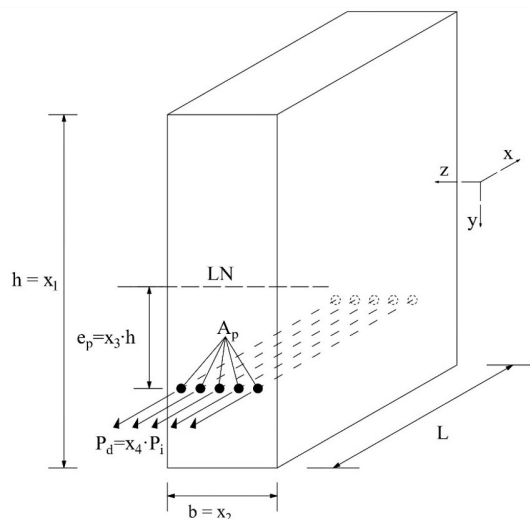


Figure 3. Cross-section of the analyzed beam

To evaluate the carbon footprint of the beam production it was taken into consideration the form work area ($A_{form\ work}$), active steel volume (V_s), concrete volume (V_c), active steel weight (P_s), concrete weight (P_c), total weight (P_{tot}) and the objective function (OF), are presented in Equations 28, 29, 30, 31, 32, 33 and 34, respectively.

$$A_{form\ work} = (2 \cdot h + b_w) \cdot L \tag{28}$$

$$V_s = A_p \cdot (L - cov) \tag{29}$$

$$V_c = b_w \cdot h \cdot L - V_s \tag{30}$$

$$P_s = V_s \cdot \gamma_s \tag{31}$$

$$P_c = V_c \cdot \gamma_c \tag{32}$$

$$P_{tot} = P_s + P_c \tag{33}$$

$$FO(x) = C_{CO2} = C_p(A_{form\ work}, P_s, V_c) + C_T(L, P_{tot}) + C_s(L) \tag{34}$$

Therefore the Objective Function presented in Equation 34 is composed of the total carbon emissions (C_{CO2}) which is given by the sum of carbon emissions generated during the production (C_p), transportation (C_T), and placement (C_s) stages of the beam, cov is the cover of the concrete beam; γ_s and γ_c are the specific weights of the active reinforcement and concrete, respectively. Further details of the carbon emission calculation function are given in section 4.5.

Table 4 presents the fixed input variables of the optimization problem, i.e., independent of the algorithm iteration, these values do not change. This procedure is common in structural engineering problems since the design engineer wants to determine the best possible geometry given fixed parameters like the temperature of the project execution site, external loads, and section model requested by the contractor (in this case, the rectangular section was adopted because it is widely used in the precast industry) and the selected concrete characteristics.

Table 4. Fixed parameters of the concrete beam design.

Parameter	Value
Slump	12 cm
Cover (cov)	3.5 cm
Coefficient of unfavorable dynamic amplification (β)	1.30
Length of the prestressing course (L_{course})	150 m
Anchorage slippage (δ_{anc})	6 mm
Frequent combination reduction factor (ψ_1)	0.4
Quasi-Permanent load Combination reduction factor (ψ_2)	0.3
Modulus of elasticity of steel (E_p)	200 GPa
Specific weight of the active reinforcement (γ_s)	78.5 kN/m ³
Specific weight of simple concrete (γ_s)	24 kN/m ³
Tensile strength of steel (f_{ptk})	1900 MPa
Design temperature	30 °C
Concrete creep and shrinkage times for each stage	1/3/15/45/100/∞ days
Steel relaxation times for each	2/4/16/46/101/∞ days
Steel yield strength (f_{yk})	1710 MPa
Steel type	NR
Type of cement	CPV-ARI
Type of prestressing	Limited prestressing (level 2)
Relative humidity (U)	70%
Length of the beam (L)	20 m
Beam compressive strength (f_{ck})	55 MPa
Type of Deferred Losses	Calculated
Distance between the production plant and the construction site (D)	50 km

The ranges of the design variables used in the beam simulation are described in Table 5.

Table 5. Range of design variables of the optimization problem.

Variable name	Variable	Range
Web height (h)	x_1	[70; 200]*
Web width (b)	x_2	[15; 60]*
Eccentricity Proportion (e_p)	x_3	[1/6; 9/20]**
Prestressing load proportion (α_{pi})	x_4	[0.85; 1.00]**

*unit in centimeters (cm) ** dimensionless unit

Table 6 presents the model of the beams studied. The relationship between live load (q) e a and the dead construction load (g_2) followed the usual prescriptions described in Santos et al. [31]. It is worth noting that load g_2 does not account for the self-weight of the element. Such consideration is made throughout the optimization process.

Table 6. Loading conditions for the simulations.

Case	g_2 (kN/m)	q (kN/m)	$\chi = q + g_2$
SIM-01	3.00	1.50	4.50
SIM-02	6.00	3.00	9.00
SIM-03	3.50	2.50	6.00
SIM-04	3.00	2.00	5.00
SIM-05	3.50	1.50	5.00
SIM-06	5.00	2.00	7.00
SIM-07	4.50	2.50	7.00
SIM-08	5.50	3.00	8.50
SIM-09	6.50	3.00	9.50
SIM-10	5.50	2.50	8.00

4.2 Bioinspired optimization algorithm

The algorithm used in this paper consists of the Firefly Algorithm (FA), which was proposed by Yang [32] and can be classified as a bioinspired probabilistic optimization. This is a population-based method. More than one particle walks through the sample space in search of the optimal feasible solution. In these methods, the concepts of the random variable are used to generate the initial population, which is a random event within limits established by the problem [32].

The theoretical source for the conception of this algorithm was inspired by the bioluminescence phenomenon and the influence of iterations between fireflies in the act of crossing. Therefore, the FA optimization method is based on the ability of fireflies to emit light and the ability of other individuals in the population to perceive this light.

When conceiving the algorithm, Yang [32] defined some precepts to help in the development, which are: all fireflies have a single gender, they are attracted to each other; the attraction capacity of each firefly is proportional to its brightness, and this decreases according to the increasing distances between individuals of the population.

With the generation of the initial populations, the firefly (or design variable) starts a random walk so that x "moves" according to an update function of the design variables (ω), as described in Equation 35, where x is the vector of design variables, ω is the update vector function of the design variable x and t is the number of iterations.

$$x^{t+1} = x^t + \omega^t \tag{35}$$

From this new direction are the new positions and possible candidate solutions for generating the optimal design point [33]. Therefore, the movement among the population of fireflies at each step of the iterative process is given by Equation 36.

$$\omega^t = \beta \cdot (x_j^t - x_i^t) + \alpha \cdot (\eta - 0.5 \cdot \epsilon) \tag{36}$$

From Equation 36, β is the attractiveness term between fireflies i and j , \mathbf{x}_i is firefly i , \mathbf{x}_j is firefly j , $\boldsymbol{\eta}$ is the vector of random numbers between 0 and 1, α is the randomness factor, and $\boldsymbol{\epsilon}$ is a unit vector.

The randomness factor α follows an exponential decay behavior according to the number of iterations t , following the formulation proposed by Equation 37, where θ is the decay constant and value equal to 0.98.

$$\alpha = \alpha_{min} + (\alpha_{max} - \alpha_{min}) \cdot \theta^t \tag{37}$$

The term β represents the attractiveness of the fireflies in the swarm. Such attractiveness is described according to Equation 38, where β_0 is the attractiveness for a distance $r = 0$, r_{ij} is a Euclidean distance between fireflies i and j (Equation 39), and γ is the light absorption parameter (Equation 40).

$$\beta = \beta_0 e^{-\gamma r_{ij}^2} \cong \frac{\beta_0}{1 + \gamma r_{ij}^2} \tag{38}$$

$$r_{ij} = \|\mathbf{x}_i - \mathbf{x}_j\| = \sqrt{\sum_{k=1}^d (\mathbf{x}_{i,k} - \mathbf{x}_{j,k})^2} \tag{39}$$

$$\gamma = \frac{1}{r^2} \tag{40}$$

$$\mathbf{r} = \mathbf{x}_{max} - \mathbf{x}_{min} \tag{41}$$

From Equations 39, 40, and 41, k is the k -th component of the vector of design variables \mathbf{x} , d is the number of design variables, \mathbf{x}_{max} is the upper bound of the design variables, \mathbf{x}_{min} is the lower bound of the design variables, and \mathbf{r} is the distance between the upper bound (\mathbf{x}_{max}) and the lower bound (\mathbf{x}_{min}).

The application of FA or any other probabilistic optimization method with population characteristics requires attention in defining the parameters of the algorithm (attractiveness: β and γ ; randomness: α).

Table 7 presents the input parameters of the FA that were based on the study by Pereira et al. [34]. In the present research, a total population of 10 individuals, randomly generated, will be considered. A total of 500 generations will be employed.

Table 7. FA input parameters.

Parameter	Meaning	Adopted value
β_0	Firefly attractiveness	0.98
N_{gen}	Number of generations	500
N_{pop}	Population size	10
α_{min}	Minimum randomness factor	0.20
α_{max}	Maximum randomness factor	0.95
R_p	Penalty factor	10^6

For this study, all simulations were evaluated 30 times to check the distribution of the optimization results.

4.3 Constraints applied to beam design and their treatment

Since this is an engineering problem, the optimization studied in this research follows the constrained optimization model. In problems of this nature, the functions that determine the constraint design conditions are relative to the limit state Equations as prescribed by ABNT NBR 6118 [25], ABNT NBR 9062 [30], and ABNT NBR 14861 [23].

The constraint Equations that determine the normative Limit States are described in Equations 42 to 45. (a) Equation 42 represents the Limit State Equations that verify the normal stresses in the design transient phases (lifting, storage, transportation, and placement) in service. σ_b and σ_t refer to the normal stress acting on the bottom and top surface, described in Equations 13 and 14 respectively. σ_{max} refers to the maximum stress allowed on the edges according to Table 2; (b) Equation 43 represents the verification of Ultimate Limit State (ULS) in bending moment,

see in section 3.3; (c) Equation 44 represents the verification of possible rupture of the compressed strut in the ULS, see in Equation 18; and (d) Finally, Equation 45 represents the verification of the deflection, considering the effects of creep, for prestressed elements. In this equation f refers to the deflection acting on the beam and f_{lim} refers to the limit deflection prescribed by the norm. The deflection calculation procedure can be seen in Equations 15 to 17.

$$\frac{\sigma_{b,t}}{\sigma_{max}} - 1 \leq 0 \quad \mathbf{g}_j, j = 1 \text{ a } 4, 10 \text{ a } 21 \tag{42}$$

$$\frac{M_{sd}}{M_{Rd}} - 1 \leq 0 \quad \mathbf{g}_j, j = 5 \tag{43}$$

$$\frac{V_{sd}}{V_{Rd2}} - 1 \leq 0 \quad \mathbf{g}_j, j = 6 \tag{44}$$

$$\frac{f}{f_{lim}} - 1 \leq 0 \quad \mathbf{g}_j, j = 7 \text{ a } 9 \tag{45}$$

As can be seen, the constraints have been normalized to avoid scaling problems within the Equations studied. This is a traditional procedure in problems of this nature, as seen in Equations 42, 43, 44, and 45.

It is worth mentioning that for this work the resistant moment (Equation 22) was limited to a ductility of 0.35 ($x/d < 0.35$) characterizing a part without compression reinforcement. Such a prescription follows the recommendation of section 14.6.4.3 of ABNT NBR 6118 [25].

For the constraint treatment procedure, the outer penalty technique was used [35], [36]. The OF is modified to obtain a pseudo-objective function, where \mathbf{g}_j represents the inequality constraints and \mathbf{h}_k the equality constraints. Equation 46 shows the adopted penalization method, and the penalized Objective Function C_{CO_2} is presented in Equation 47.

$$P(\mathbf{x}) = \sum_{j=1}^m \max[0, \mathbf{g}_j(\mathbf{x})]^2 + \sum_{k=1}^n [\mathbf{h}_k(\mathbf{x})]^2 \tag{46}$$

$$C_{CO_2}(\mathbf{x}) = FO(\mathbf{x}) + R_p \cdot P(\mathbf{x}) \tag{47}$$

From Equation 47, it is worth noting that $P(\mathbf{x})$ is the static exterior penalty function, j, k is j -th inequality constraint and k -th equality constraint, respectively, m, n are the total number of inequality and equality constraints, respectively, \mathbf{x} is the solution vector (random population), \mathbf{g}, \mathbf{h} are the set of inequality and equality constraints, and $C_{CO_2}(\mathbf{x})$ is the penalized objective function.

4.4 Characterization of the optimization problem

Figure 4 presents the complete operation of the Objective Function for each particle in the swarm, i.e., each individual in the population will have a single solution set ($\mathbf{x}^T = []_{1 \times 4}$) over a single iteration and this changes with each movement of the population.

In stage 1 (Flowchart see Figure 4) of the Objective Function the geometric and material properties are determined for all project stages. These are (a) Cable Cutting, (b) Storage, (c) Transportation, (d) Assembly, and (e) Service.

After determining all geometric and mechanical properties, the definition of a longitudinal prestressing tendon reinforcement (A_p) was performed in stage 2. Therefore, the variable A_p is a state variable that changes for each particle and each population movement of the algorithm. This procedure consisted in establishing which steel area was necessary to satisfy the axial edge tensioning condition in service. The choice of a longitudinal reinforcement via a Serviceability Limit State (SLS) is a resource widely used by design professionals since this limit state is usually predominate over other limit states. This recommendation can be seen in Cholfe and Bonilha [37], Carvalho [38], and Rodrigues [39]. Once the longitudinal tendon reinforcement is determined, it is possible to determine the prestressing losses still in stage 2. This research calculates prestressing losses as established in ABNT NBR 6118 [25] and its annexes.

After determining the tendon reinforcement, the subsequent stages 3 to 5 verify the design constraints as explained in Equations 42 to 45. In stage 6 of the algorithm, the penalty method considers the engineering problem with constraints.

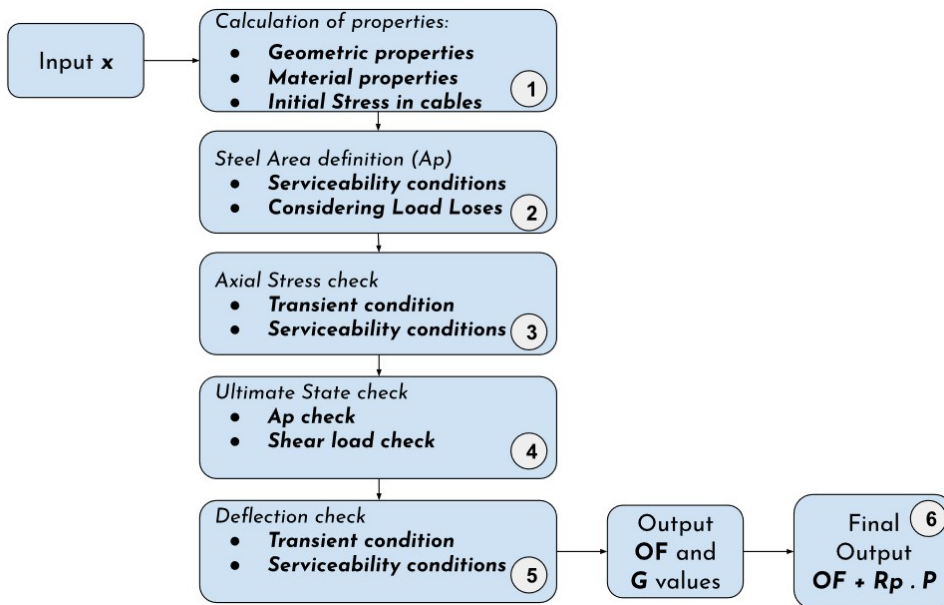


Figure 4. Flowchart of the objective function.

4.5 Carbon Emission Model

The total carbon emissions in the construction process of precast components are the sum of the emissions during the production, transportation, and placement stages. The calculation model follows the proposition of Yepes et al. [1], as shown in Equation 48:

$$C_{CO2} = C_P + C_T + C_S \tag{48}$$

Where C_{CO2} represents the total carbon emissions generated in the precast component construction process, C_P , C_T , and C_S represent the carbon emissions generated during production, transportation, and placement stages, respectively.

4.5.1 Production Stage

The carbon emissions generated during the precast elements production stage come from raw materials, fuel oil, and electrical energy consumed during production. The calculation model is shown in Equation 49:

$$C_P = \sum_{i=1}^n (A_{form\ work} \cdot F_{fw} + P_s \cdot F_s + V_c \cdot F_c) \tag{49}$$

Where C_P represents the total carbon emissions generated during the production phase of the precast element; n indicates the type of precast component. F_{fw} , F_s , e F_c represent the carbon emission coefficients for the work form, prestressing tendon reinforcement, and concrete during the production stage, respectively.

To determine the carbon emission coefficients, they were defined according to the procedures proposed by Yepes et al. [1]. It was assumed steel with production via electric arc furnace (EAF), approximately 40% recycled steel scrap. The coefficients F_{fw} , F_s , and F_c can be obtained in Table 8.

Table 8. Unit CO₂ emission of the beam in the production stage [1].

Description	CO ₂ emission (kg CO ₂ /unit)	unit
Active steel	5.64	kg
Beam formwork	2.24	m ²
Beam concrete C-35	263.96	m ³
Beam concrete C-40	298.57	m ³
Beam concrete C-45	330.25	m ³
Beam concrete C-50	358.97	m ³
Beam concrete C-55	384.76	m ³
Beam concrete C-60	407.59	m ³
Beam concrete C-70	444.43	m ³
Beam concrete C-80	469.49	m ³
Beam concrete C-90	482.77	m ³
Beam concrete C-100	484.27	m ³

4.5.2 Transportation stage

The carbon emissions generated during the transportation stage of the precast elements are mainly from the exhaust emissions of the transport vehicles. The calculation model is shown in Equation 50:

$$C_T = \sum_{i=1}^n \left(F_T \cdot P_{tot} \cdot \frac{D}{50} \right) \tag{50}$$

Where C_T represents the total carbon emissions generated during the transportation stage of the precast components, n represents the number of vehicles required to transport the precast components, F_T represents the carbon emission coefficient of transportation (kg CO₂/t) on the truck when transporting a beam of length L , and D represents the distance between the production plant and the construction site in km. It should be noted that the transportation of the beams was considered separately, and the carbon emission coefficients in transportation can be obtained in Table 9 since this depends on the length of the beam.

Table 9. CO₂ emissions from beam transportation stage (distance up to 50 km, one way) [1].

Maximum beam length (m)	Transport emission (kg CO ₂ /t)
20	76.38
25	80.12
30	98.25
35	95.38
40	93.00

4.5.3 Placement stage

The carbon emissions generated during the placement stage of the precast components come mainly from the following three aspects: raw materials, fuel oil, and electrical energy consumed during installation. The calculation model is shown in Equation 51:

$$C_S = \sum_{i=1}^n (L \cdot F_S) \tag{51}$$

Where C_S represents the total carbon emissions generated during the installation phase of precast components; n indicates the type of precast components. F_S represents the carbon emission coefficient at the placement stage (kg CO₂/m) for a beam of length L . It should be noted that the placement of the beams was considered separately, and the carbon emission coefficients at the assembly stage can be obtained from Table 10 since this depends on the length of the beam.

Table 10. CO₂ emissions from beam placement stage(distance up to 50 km, one way) [1].

Maximum beam length (m)	Placement emission (kg CO ₂ /m)
20	39.43
25	50.24
30	61.05
35	65.18
40	69.31

5 RESULTS AND DISCUSSION

In this section, the results of the optimization tests focused on the study of prestressed precast concrete beams are presented. As presented in section 4, the beams employed for this paper have a rectangular cross-section with a straight cable.

Table 11 presents the statistical values of the 30 executions of the optimization algorithm for the different types of beams considered. Figure 5 presents graphically the answers to the optimization process for the simulations, in this case, the minimum carbon emission value.

It is possible to verify through Table 11 that the optimization process presented a feasibility rate (FR) of 100% for all simulations. The answers of the 30 executions of each simulation found beams that respected all the design constraints informed for this problem.

In terms of CO₂ emission, the beams studied in this work presented an average carbon emission of 3282.59 kg, with the emission increasing according to the load imposed on the structural element. Therefore, the highest carbon emission was equivalent to the highest load given in the SIM-09 simulation. For this simulation, the total loading of 9.50 kN/m resulted in carbon emission of 3630.52 kg. The lowest carbon emission was for simulation SIM-01 with 2910.67 kg for a loading of 4.50 kN/m.

The carbon emission increased on average by about 723.01 kg between the minimum and maximum loading values. In order to mathematically represent this data set, a linear regression from the Scikit-Learn library was employed. The Equation representing this set is given by $2286.40 + 143.34 \cdot \chi$ with an $R^2 = 0.998$.

Table 11. Range of design variables for the optimization problem.

Case	$C_{CO2_{max}}$ (kg)	$C_{CO2_{min}}$ (kg)	μ (kg)	σ (kg)	FR (%)
SIM-01	2932.16	2910.67	2919.91	5.17	100
SIM-02	3604.59	3573.47	3584.36	8.80	100
SIM-03	3170.93	3150.88	3159.89	14.11	100
SIM-04	3023.86	3005.18	3013.41	5.38	100
SIM-05	3020.04	3002.77	3010.93	4.70	100
SIM-06	3325.60	3302.23	3316.57	5.68	100
SIM-07	3329.89	3307.11	3317.96	6.28	100
SIM-08	3538.36	3506.75	3517.15	7.71	100
SIM-09	3657.11	3630.52	3642.92	7.20	100
SIM-10	3470.89	3436.35	3451.99	8.33	100

C_{CO2} – CO₂ emission; μ – Mean of results; σ – Standard deviation of results; FR – feasibility rate of the optimization

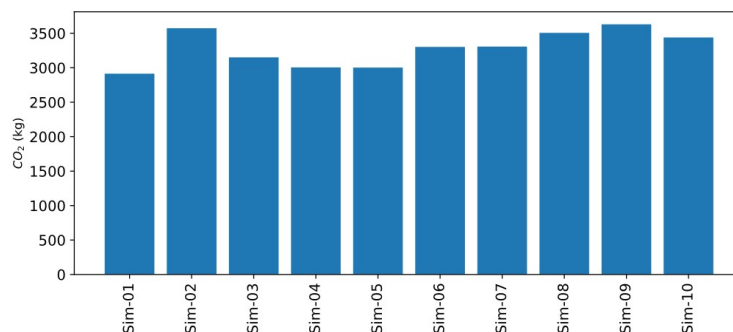


Figure 5. Carbon emission of the beams as a function of simulation.

The convergence results of the best response among the 30 repetitions are illustrated in Figure 6. It can be seen that the results show a convergence pattern from 10^3 number of evaluations of the Objective Function (NEOF).

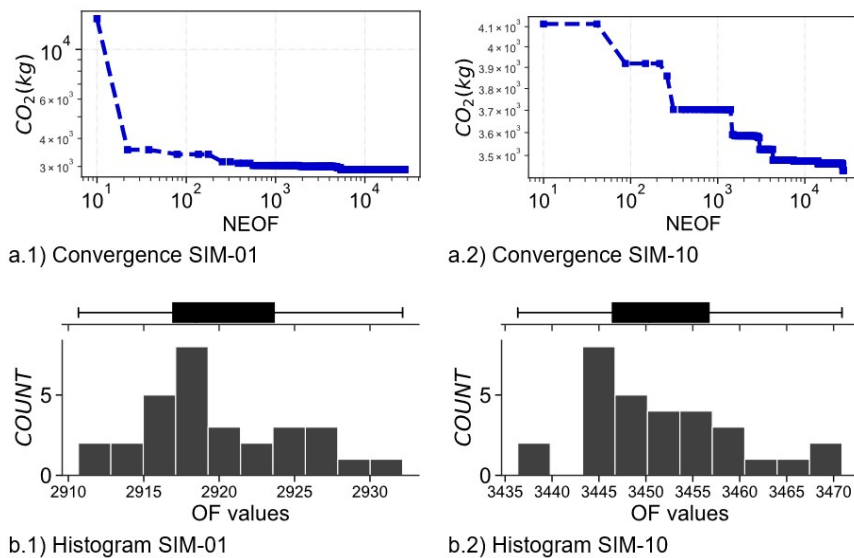


Figure 6. Result of the optimization process a) Convergence kg vs. Number of Evaluations of the Objective Function (NEOF); b) Histogram of the 30 repetition runs.

Figure 7 presents the set of constraints for the optimal response for all simulations presented in this study. It is possible to see that the limiting design constraints are the ultimate limit state (ULS) for the resistant moment (g_5) and the normal stress constraints for a serviceability limit state (SLS) in transient situations (g_{11}). In the case of these two constraints, they reached the limit $g_j = 0$ in some of the simulations.

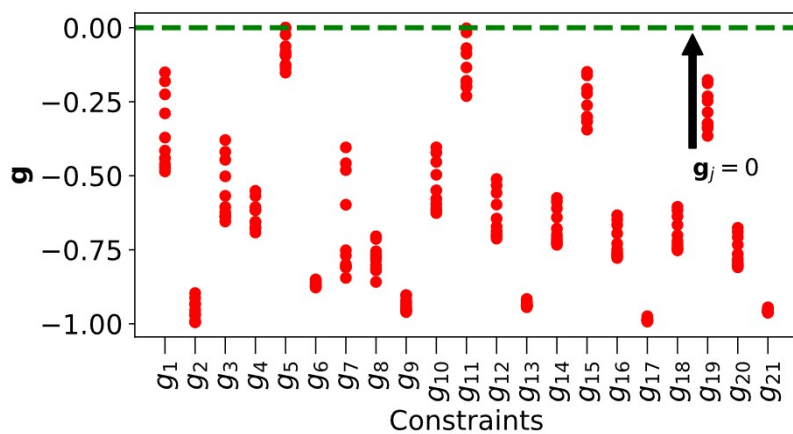


Figure 7. Evaluation of the constraints for the optimal response in simulations 01 to 10.

6 CONCLUSIONS

Firstly, it is possible to state that the optimization algorithm employed was able to be used as a tool to optimize a structural design (feasibility rate higher than 90%) of precast and prestressed beams. This fact corroborates the statement that optimization techniques can be good alternatives for structural design. Remember that the algorithm will never replace the design engineer, but it will contribute as a tool in developing a design's structure process.

Regarding carbon emission it is possible to verify a relationship between the increase of emission and the load, since elements with greater inertia tend to emit a greater amount of CO₂. It is possible to verify by the convergence diagrams in Figure 6 that the optimization process effectively reduced the carbon emission of the beams considering the design constraints imposed by ABNT NBR 6118 [25]. Besides that, the optimization process was effective in relation to the range of dimensions proposed in Table 5.

Beyond presenting a tool that enables the optimal sizing of concrete elements, the work also looks at the issue of CO₂ emission evaluation during the execution of a structural project. In this sense, the authors present some suggestions for the development of future works focused on this analysis of carbon emission in structural design:

- Development of cost functions that address not only the structural weight but also the carbon credit;
- Consideration of other structural elements as for example hollow core slabs;
- Construction of carbon emission charts as a function of load and material properties.

ACKNOWLEDGEMENTS

We would like to acknowledge the Coordenação de Aperfeiçoamento de Pessoal de Nível Superior – Brasil (CAPES) – Finance Code 001

REFERENCES

- [1] V. Yepes, J. V. Martí, and T. García-Segura, "Cost and CO₂ emission optimization of precast–prestressed concrete U-beam road bridges by a hybrid glowworm swarm algorithm," *Autom. Construct.*, vol. 49, pp. 123–134, Jan. 2015., <http://dx.doi.org/10.1016/j.autcon.2014.10.013>.
- [2] United Nations Environment Programme, "Global status report for buildings and construction: towards a zero-emission, efficient and resilient buildings and construction sector," Nairobi, Kenya: United Nations Environment Programme, Dec. 2020. https://globalabc.org/sites/default/files/inline-files/2020%20Buildings%20GSR_FULL%20REPORT.pdf (accessed Mar. 29, 2022).
- [3] E. Worrell, L. Price, N. Martin, C. Hendriks and L. O. Meida, "Carbon dioxide emissions from the global cement industry," *Annu. Rev. Energy Environ.*, vol. 26, pp. 303–329, Nov. 2001, <http://dx.doi.org/10.1146/annurev.energy.26.1.303>.
- [4] H. Su, Q. Su, C. Xu, X. Zhang, and D. Lei, "Shear performance and dimension rationalization study on the rubber sleeved stud connector in continuous composite girder," *Eng. Struct.*, vol. 240, pp. 112371, Aug. 2021, <http://dx.doi.org/10.1016/j.engstruct.2021.112371>.
- [5] G. L. Vatulia, O. V. Lobiak, S. V. Deryzemlia, M. A. Verevicheva and Y. F. Orel, "Rationalization of cross-sections of the composite reinforced concrete span structure of bridges with a monolithic reinforced concrete roadway slab," in *IOP Conf. Ser.: Mater. Sci. Eng.*, vol. 664, no. 1, p. 012014, Oct. 2019, doi: 10.1088/1757-899X/664/1/012014.
- [6] O. Petrova, O. Lugchenko, M. Hammud, and A. Nazhem "To the rationalization of the constructive solutions of the bridge supports," in *MATEC Web Conf.*, vol. 116, p. 02025, 2017, doi: 10.1051/mateconf/201711602025.
- [7] L. L. Wagner, A. L. S. Corrêa, and D. B. de Freitas, "Review on the use of prefabricated elements," *B.J.D.*, vol. 6, no. 10, pp. 75455–75465, 2020, <http://dx.doi.org/10.34117/bjdv6n10-103>.
- [8] J. Navarro-Rubio, P. Pineda, and A. García-Martínez, "Sustainability, prefabrication and building optimization under different durability and re-using scenarios: potential of dry precast structural connections," *Sustain. Cities Soc.*, vol. 44, pp. 614–628, Jan. 2019, <http://dx.doi.org/10.1016/j.scs.2018.10.045>.
- [9] R. F. Vasconcelos, "Otimização de elementos pré- moldados de concreto: lajes alveolares e vigas com cabo reto," M.S. thesis, Fed. Univ. Goiás, Goiânia, GO, 2014. [Online]. Available: <http://repositorio.bc.ufg.br/tede/handle/tede/5678>
- [10] S. K. Azad, M. Bybordiani, S. K. Azad, and F. K. J. Jawad, "Simultaneous size and geometry optimization of steel trusses under dynamic excitations," *Struct. Multidiscipl. Optim.*, vol. 58, no. 6, pp. 2545–2563, Dec 2018., <http://dx.doi.org/10.1007/s00158-018-2039-7>.
- [11] A. S. Al-Gahtani, S. S. Al-Saadoun, and E. A. Abul-Feilat, "Design optimization of continuous partially prestressed concrete beams," *Comput. Struc.*, vol. 55, no. 2, pp. 365–370, Apr. 1995, [http://dx.doi.org/10.1016/0045-7949\(94\)00481-H](http://dx.doi.org/10.1016/0045-7949(94)00481-H).
- [12] V. Albero, H. Saura, A. Hospitaler, J. M. Montalvã, and M. L. Romero, "Optimal design of prestressed concrete hollow core slabs taking into account its fire resistance," *Adv. Eng. Softw.*, vol. 122, pp. 81–92, Aug. 2018, <http://dx.doi.org/10.1016/j.advengsoft.2018.05.001>.
- [13] V. C. Castilho, "Optimization of precast prestressed elements using genetic algorithms," Ph.D. Thesis, Univ. São Paulo, São Carlos, SP, 2003. <http://dx.doi.org/10.11606/T.18.2003.tde-14102003-113629>.
- [14] V. C. Castilho, M. C. Nicoletti, and M. K. El Debs, "An investigation of the use of three selection-based genetic algorithm families when minimizing the production cost of hollow core slabs," *Comput. Methods Appl. Mech. Eng.*, vol. 194, no. 45–47, pp. 4651–4667, Nov. 2005, <http://dx.doi.org/10.1016/j.cma.2004.12.008>.

- [15] M. A. Juliani and W. J. S. Gomes, "Optimal configuration of RC frames considering ultimate and serviceability limit state constraints," *Rev. IBRACON Estrut. Mater.*, vol. 14, no. 2, pp. e14204, 2021, <http://dx.doi.org/10.1590/s1983-41952021000200004>.
- [16] S. L. Pires and M. C. A. T. da Silva, "Optimization of slender reinforced concrete columns subjected to biaxial bending using genetic algorithms," *Rev. IBRACON Estrut. Mater.*, vol. 14, no. 6, pp. e14610, 2021., <http://dx.doi.org/10.1590/s1983-41952021000600010>.
- [17] E. U. Cardoso, R. Q. Rodríguez, L. Q. Machado, F. F. Kunz, P. S. Santos and A. P. C. Quispe, "Structural optimization of concrete plane frames considering the static and dynamic wind effect," *Rev. IBRACON Estrut. Mater.*, vol. 15, no. 1, pp. e15109, 2021, <http://dx.doi.org/10.1590/s1983-41952022000100009>.
- [18] A. L. Christoforo, M. H. M. de Moraes, I. F. Fraga, W. M. Pereira Junior, and F. A. R. Lahr, "Computational intelligence applied in optimal design of wooden plane trusses," *Eng. Agric.*, vol. 42, no. spe, pp. e20210123, 2022, <http://dx.doi.org/10.1590/1809-4430-eng.agric.v42nepe20210123/2022>.
- [19] M. H. M. Moraes, I. F. Fraga, W. M. Pereira Junior, and A. L. Christoforo, "Comparative analysis of the mechanical performance of timber trusses structural typologies applying computational intelligence," *Rev. Arvore*, vol. 46, pp. e4604, 2022, <http://dx.doi.org/10.1590/1806-908820220000004>.
- [20] M. Yücel, S. M. Nigdeli, and G. Bekdaş, "Generation of sustainable models with multi-objective optimum design of reinforced concrete (RC) structures," *Structures*, vol. 40, pp. 223–236, Jun. 2022, <http://dx.doi.org/10.1016/j.istruc.2022.04.020>.
- [21] R. Yu, D. Zhang, and H. Yan, "Embodied energy and cost optimization of RC beam under blast load," *Math. Probl. Eng.*, vol. 2017, pp. 1–8, 2017, <http://dx.doi.org/10.1155/2017/1907972>.
- [22] R. Yu, L. Chen, D. Zhang, and Z. Wang, "Life cycle embodied energy analysis of RC structures considering chloride-induced corrosion in seismic regions," *Structures*, vol. 25, pp. 839–848, Jun. 2020, <http://dx.doi.org/10.1016/j.istruc.2020.03.049>.
- [23] Associação Brasileira de Normas Técnicas, *Lajes Alveolares Pré-moldadas de Concreto Protendido — Requisitos e Procedimentos*: NBR 14861, 2011.
- [24] Associação Brasileira de Normas Técnicas, *Projeto e Execução de Estruturas de Concreto Pré-moldado*: NBR 9062, 2017.
- [25] Associação Brasileira de Normas Técnicas, *Projeto de Estruturas de Concreto — Procedimento*, NBR: 6118, 2014.
- [26] G. B. Borghi, G. D. P. Lisboa, and D. D. L. Araújo, "Analysis of lateral stability of precast concrete beams for bridges in transitory phases," *REEC*, vol. 15, no. 1, Oct. 2018, <http://dx.doi.org/10.5216/reec.v15i1.49640>.
- [27] B. Lewicki, *Edifícios de Viviendas Prefabricadas con Elementos de Grandes Dimensiones*. Madrid: Insituto Eduardo Torroja de la Construcción y del Cemento, 1968.
- [28] P. A. Krah, M. C. V. Lima, and M. K. El Debs, "Recommendations for verifying lateral stability of precast beams in transitory phases," *Rev. IBRACON Estrut. Mater.*, vol. 8, no. 6, pp. 763–774, Dec. 2015, <http://dx.doi.org/10.1590/S1983-41952015000600003>.
- [29] D. A. Sheppard and W. R. Phillips, *Plant-Cast Precast and Prestressed Concrete: A Design Guide*. New York: McGraw-Hill, 1989.
- [30] Associação Brasileira de Normas Técnicas, *Projeto e Execução de Estruturas de Concreto Pré-moldado*, NBR 9062, 2017.
- [31] D. M. Santos, F. R. Stucchi, and A. T. Beck, "Reliability of beams designed in accordance with Brazilian codes," *Rev. IBRACON Estrut. Mater.*, vol. 7, pp. 723–746, Oct. 2014, <http://dx.doi.org/10.1590/S1983-41952014000500002>.
- [32] X.-S. Yang, *Nature-Inspired Metaheuristic Algorithms*. Frome: Luniver Press, 2008.
- [33] H. Wang et al., "Firefly algorithm with neighborhood attraction," *Inf. Sci.*, vol. 382–383, pp. 374–387, Mar. 2017, <http://dx.doi.org/10.1016/j.ins.2016.12.024>.
- [34] L. L. M. Pereira et al., "Estudo de sensibilidade do algoritmo de colônia de vagalumes para um problema de engenharia envolvendo dimensionamento de treliças," *Tend. Mater. Apl. Comput.*, vol. 21, no. 3, pp. 583, Nov. 2020, <http://dx.doi.org/10.5540/tema.2020.021.03.583>.
- [35] A. F. Kuri-Morales and J. Gutiérrez-García, "Penalty function methods for constrained optimization with genetic algorithms: a statistical analysis," in *MICAI 2002: Advances in Artificial Intelligence*, Berlin, Heidelberg, 2002, pp. 108–117. http://dx.doi.org/10.1007/3-540-46016-0_12.
- [36] Ö. Yeniay, "Penalty function methods for constrained optimization with genetic algorithms," *Math. Comput. Appl.*, vol. 10, no. 1, pp. 45–56, 2005, <http://dx.doi.org/10.3390/mca10010045>.
- [37] L. Cholfé and L. Bonilha, *Concreto Protendido: Teoria e Prática*. 2a ed. São Paulo: Editora Oficina de Textos, 2018.
- [38] R. C. Carvalho, *Estruturas em Concreto Protendido*. 2a ed. São Paulo: Pini, 2017.
- [39] C. Rodrigues, "Sistematização do cálculo e verificação de sistemas estruturais de galpões pré-fabricados de concreto," M.S. thesis, Univ. Fed. São Carlos, São Carlos, SP, 2012.

Author contributions: MHMM: Writing, Development, Analyses; WMPJr: Supervision, Development, Analysis; SRMA: Supervision, Development, Analysis; GMGF: Writing, Development, Analysis; RFV: Writing, Development.

Editors: Edna Possan, Mark Alexander